USGS
science for a changing world
U.S. DEPARTMENT OF THE INTERIOR
U.S. GEOLOGICAL SURVEY

Prepared for the
NATIONAL AERONAUTICS AND SPACE ADMINISTRATION

STRUCTURE/VOLCANO MAP OF THE KAIWAN FLUCTUS QUADRANGLE (V–44), VENUS

By
Nathan T. Bridges and George E. McGill
2002

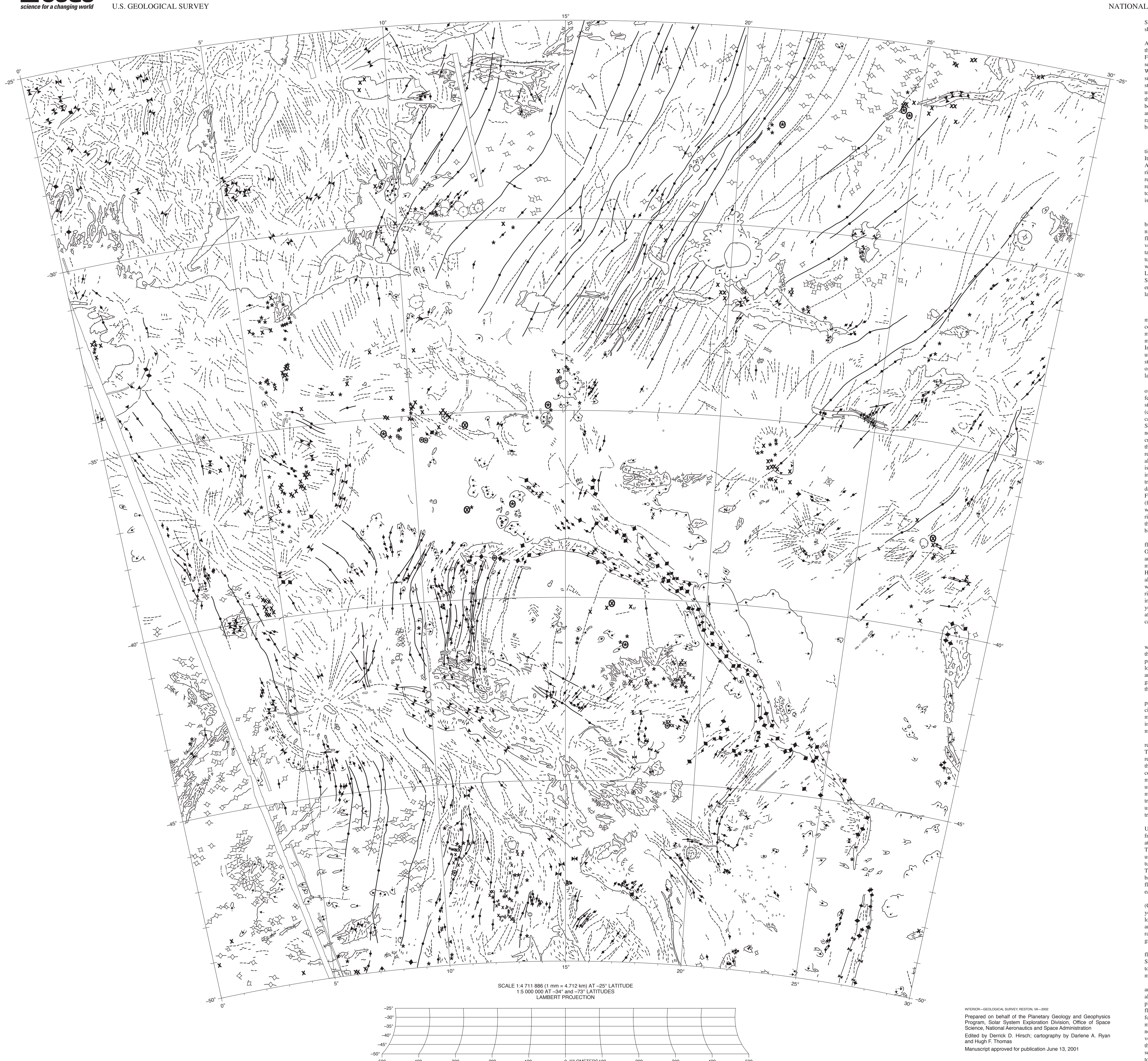

SCALE 1:4 711 886 (1 mm = 4.712 km) AT −25° LATITUDE
1:5 000 000 AT −34° and −73° LATITUDES
LAMBERT PROJECTION

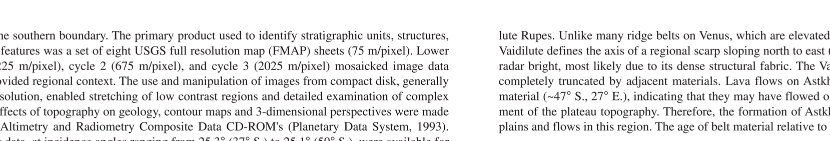

INTERIOR—GEOLOGICAL SURVEY, RESTON, VA—2002

Prepared on behalf of the Planetary Geology and Geophysics Program, Solar System Exploration Division, Office of Space Science, National Aeronautics and Space Administration

Edited by Derrick D. Hirsch; cartography by Darlene A. Ryan and Hugh F. Thomas

Manuscript approved for publication June 13, 2001

The Magellan Mission

The Magellan spacecraft orbited Venus from August 10, 1990, until it plunged into the venusian atmosphere on October 12, 1994. Magellan had the objectives of (1) improving knowledge of the geologic processes, surface properties, and geologic history of Venus by analysis of surface radar characteristics, topography, and morphology and (2) improving knowledge of the geophysics of Venus by analysis of venusian gravity.

The Magellan spacecraft carried a 12.6-cm radar system to map the surface of Venus. The transmitter and receiver systems were used to collect three datasets: synthetic aperture radar (SAR) images of the surface, passive microwave thermal emission observations, and measurements of the backscattered power at small angles of incidence, which were processed to yield altimetric data. Radar imaging and altimetric and radiometric mapping of the venusian surface were done in mission cycles 1, 2, and 3, from September 1990 until September 1992. Ninety-eight percent of the surface was mapped with radar resolution of approximately 120 meters. The SAR observations were projected to a 75-m nominal horizontal resolution; these full-resolution data compose the image base used in geologic mapping. The primary polarization mode was horizontal-transmit, horizontal-receive (HH), but additional data for selected areas were collected for the vertical polarization sense. Incidence angles varied from about 20° to 45°.

High-resolution Doppler tracking of the spacecraft was done from September 1992 through October 1994 (mission cycles 4, 5, 6). High-resolution gravity observations from about 950 orbits were obtained between September 1992 and May 1993, while Magellan was in an elliptical orbit with a periapsis near 175 kilometers and an apoapsis near 8,000 kilometers. Observations from an additional 1,500 orbits were obtained following orbit-circularization in mid-1993. These data exist as a 75° by 75° harmonic field.

Magellan Radar Data

Radar backscatter power is determined by the morphology of the surface at a broad range of scales and by the intrinsic reflectivity, or dielectric constant, of the material. Topography at scales of several meters and larger can produce quasi-specular echoes, with the strength of the return greatest when the local surface is perpendicular to the incident beam. This type of scattering is most important at very small angles of incidence, because natural surfaces generally have few large tilted facets at high angles. The exception is in areas of steep slopes, such as ridges or rift zones, where favorably tilted terrain can produce very bright signatures in the radar image. For most other areas, diffuse echoes from roughness at scales comparable to the radar wavelength are responsible for variations in the SAR return. In either case, the echo strength is also modulated by the reflectivity of the surface material. The density of the upper few wavelengths of the surface can have a significant effect. Low-density layers, such as crater ejecta or volcanic ash, can absorb the incident energy and produce a lower observed echo. On Venus, a rapid increase in reflectivity exists at a certain critical elevation, above which high-dielectric minerals or coatings are thermodynamically stable. This effect leads to very bright SAR echoes from virtually all areas above that critical elevation.

The measurements of passive thermal emission from Venus, though of much lower spatial resolution than the SAR data, are more sensitive to changes in the dielectric constant of the surface than to roughness. As such, they can be used to augment studies of the surface and to discriminate between roughness and reflectivity effects. Observations of the near-nadir backscatter power, collected using a separate smaller antenna on the spacecraft, were modeled using the Hagfors expression for echoes from gently undulating surfaces to yield estimates of planetary radius, Fresnel reflectivity, and root-mean-square (rms) slope. The topography data produced by this technique have horizontal footprint sizes of about 10 km near periapsis and a vertical resolution of approximately 100 m. The Fresnel reflectivity data provide a comparison to the emissivity maps, and the rms slope parameter is an indicator of the surface tilts, which contribute to the quasi-specular scattering component.

INTRODUCTION

Kaiwan Fluctus quadrangle (V–44), Venus, lies between 25° to 50° S. latitude and 0° to 30° E. longitude. Alpha Regio dominates the northwestern part of the quadrangle. This Greenland-sized block of tessera has pronounced topography, rising up to 3 km above the surrounding plains (fig. 1) (Bindschadler and others, 1992). The south-central to southeastern part of the quadrangle contains Astkhik Planum, which stands a few hundred meters above the adjacent plains (see discussion of Derceto Plateau in Baer and others, 1994). The southwest margin of Astkhik is bounded by tessera material, whereas the northern and eastern edges are surrounded by a belt of ridges and troughs that slope away from the plateau into a topographic moat. Seven coronae are in V–44; five of these—Eve, Carpo, Tamfana, Selu, and Derceto—are part of a larger extensional belt that continues southward into V–56 quadrangle (Baer and others, 1994). A classic assemblage of steep-sided domes, Seoritsu Farra, is 200 km east of Alpha Regio (Pavri and others, 1992). The map area contains 15 impact craters, including Stuart, which is recognized for its extensive impact melt outflows (Asimow and Wood, 1992) and parabolic halo (Schultz, 1992).

DATA SOURCES AND METHODOLOGY

The map base is a 1:5 million scale U.S. Geological Survey (USGS) mosaic made from cycle 1 Magellan synthetic aperture radar (SAR) images. Radar incidence angles range from 35.5° at the northern boundary of the map to 23.1° at the southern boundary. The primary product used to identify stratigraphic units, structures, and other interesting features was a set of eight USGS full resolution map (FMAP) sheets (75 m/pixel). Lower resolution cycle 1 (225 m/pixel), cycle 2 (675 m/pixel), and cycle 3 (2025 m/pixel) mosaicked image data records (MIDR's) provided regional context. The use and manipulation of images from compact disk, generally at full and cycle 1 resolution, enabled stretching of low contrast regions and detailed examination of complex areas. To assess the effects of topography on geology, contour maps and 3-dimensional perspectives were made using data from the Altimetry and Radiometry Composite Data CD-ROM's (Planetary Data System, 1993). Cycle 2 right-looking data, at incidence angles ranging from 25.3° (37° S.) to 25.1° (50° S.), were available for most of the southeast quadrant of the map area. These data, together with USGS pseudo-stereo images over the whole map area, aided in visual interpretation of topography. Elevation, emissivity, root mean square slope, and Fresnel reflectivity were computed for each map unit using the Venus Ancillary Data Program (Campbell, 1995).

The geologic map (sheet 1) portrays geologic units and major structures. Geologic units were identified on the basis of radar brightness, internal fabric and structure, and superposition. Major structures were recognized by narrow radar-brightness patterns distinct from the surrounding terrain. These include radial and circumferential structures that make up parts of coronae.

A separate map (sheet 2) was prepared showing fine details of structural geology and the distribution of volcanic landforms. The structures identified include grabens, thrust faults or ramps, scarps, ridge crests, troughs, and craters. Volcanic or probable volcanic features include sinuous rilles, pits, pit chains, domes, and small shields. Small domes and shields are mapped and the presence of pits or calderas on their flanks and summits noted.

Superficial crater haloes were identified by their radar-dark interior, boundaries that crosscut geologic units and features, and a pattern that fans asymmetrically west from the parent crater. Haloes associated with the craters Stuart (Schultz, 1992) and Zenobia are shown in figure 2.

STRATIGRAPHY

Map unit classifications are divided on the basis of radar brightness and morphology. Radar-bright regions having a dense fabric of lineaments, ridges, or grooves are classified as belt and tessera materials. Digitate to lobate forms geographically isolated or associated with specific physiographic features are classified as flow materials. Circular to semi-circular features that exhibit pronounced topography or that contain radially symmetric digitate to lobate forms are divided into volcanic construct materials; these are classified separately from flow materials as they represent a distinct type of volcanic style that forms an individual edifice. Somewhat homogeneous, areally extensive regions are mapped as plains materials. Structural depressions within raised rims and commonly surrounded by radially distributed heterogeneous and digitate to lobate materials are classified as impact crater materials. In the following sections, where stratigraphy is discussed, emphasis is placed on evidence for age relationships between adjacent units in the stratigraphic column. Quantitative SAR properties for each map unit are presented in figure 3.

BELT AND TESSERA MATERIALS

Tessera material (unit t) displays pronounced and dense arrays of approximately orthogonal intersecting lineaments, ridges, and grooves. Dark material lies between and among many of these linear structures. Tessera material is present in two main blocks within the map area: Alpha Regio in the northwest and Tyche Tessera in the south. Numerous inliers of tessera material also are present throughout the map area. Tessera material is radar bright, with some of the highest SAR echoes in the whole map area (fig. 3*B*). Most likely, this radar brightness is caused by its intense structural fabric and not by its intrinsic material properties.

Abundant evidence shows that tessera material is an old unit. The density of orthogonal structures, both compressional and extensional, within the unit indicates intense deformation in a changing stress field. Structural fabrics superimposed on tessera material are truncated at plains boundaries, strongly suggesting that most of the deformation ceased before regional plains embayment. Plains materials in many cases occupy structural basins at tessera margins and in the tessera interior. These observations indicate that, where stratigraphic relations are discernible, tessera material is older than adjacent plains materials. However, three lines of evidence indicate that tessera deformation waned rather than ceased abruptly. First, three craters—Nadia, Teresa, and Virga—within or on the margins of tessera material show minor degrees of tectonism. Although Nadia shows some evidence of tectonism, its ejecta appears to lie on top of the ridged plains unit, indicating that most structural deformation in this area occurred before impact. Previous global studies found Teresa and Virga to be deformed (Schaber and others, 1995; Herrick and others, 1997; Gilmore and others, 1997), whereas only Herrick and others (1997) identified Nadia as a deformed crater. Second, some plains material slopes upward toward the margins of some adjacent tessera material, and both units share structures. Third, intratessera plains both truncate and share tessera structures. All of these observations indicate that tessera formation waned rather than ceased abruptly and that uplift and deformation modified adjacent plains. Different blocks of tessera material may not have formed at the same time, but all of them certainly are older than adjacent materials. The characteristics of tessera material before deformation cannot be determined.

Belt material (unit b) is distinguished by a densely lineated fabric of ridges and grooves areally confined within long bands at the northern and eastern margins of Astkhik Planum. This belt system is known as Vaidilute Rupes. Unlike many ridge belts on Venus, which are elevated above the surrounding plains on either side, Vaidilute defines the axis of a regional scarp sloping north to east (fig. 1). Like tessera material, belt material is radar bright, most likely due to its dense structural fabric. The Vaidilute Rupes scarp/ridge belt is old, as it is completely truncated by adjacent materials. Lava flows on Astkhik Planum trend toward a break in the belt material (~47° S., 27° E.), indicating that they may have flowed over and covered Vaidilute after the establishment of the plateau topography. Therefore, the formation of Astkhik Planum and the belt material predate the plains and flows in this region. The age of belt material relative to tessera material cannot be established.

PLAINS MATERIALS

Overview

As with most of Venus, plains materials in the map area are the most areally extensive class of stratigraphic unit. As such, they provide an important record of tectonic and volcanic processes in the map area. The plains materials are divided into nine units. The unit names are based on dominant surface characteristics (for example, ridged plains material), despite the fact that stratigraphic distinctions are primary discriminators among units. Because internal fabric and other unit characteristics are commonly gradational, a given name does not necessarily define a unit everywhere.

Densely ridged plains material is probably the oldest unit. Intratessera plains material could be just as old or older, but because it only borders tessera material, its age relative to other plains units is unknown. The edifice, ridged, and tessera-adjacent textured plains materials have ages between those of the densely ridged and textured regional plains. The remaining plains units exhibit a clear stratigraphy, with regional lineated plains material overlying the textured regional plains. The homogeneous and digitate plains material caps this sequence. Below, each plains unit is discussed, and justification is given for the assigned stratigraphic position, with age relationships relative to other materials described.

Densely Ridged Plains Material

The densely ridged plains material (unit pdr) contains regions of concentrated structural features such as ridges, grabens, and lineaments. Although the structures are a characteristic of this unit, they do not define it in all places. In many cases, areas with many structures grade into those with fewer or none. The densely ridged plains material covers a significant portion of the exposed surfaces of coronae in the Alpha-Lada chain, is adjacent to tessera material, and forms inliers throughout the map area. The densely ridged plains material makes up the oldest preserved surfaces of Eve, Carpo, Tamfana, and Selu Coronae. The structures within the unit are more densely concentrated than those in the ridged plains material (unit pr) and are oriented orthogonally near tessera material and radially or circumferentially within coronae. Unlike tessera material, the structural fabric in the densely ridged plains material is generally stronger in one orientation. Boundaries between tessera material and densely ridged plains material are indistinct and are shown as dashed lines on the geologic map, indicating that some parts of the densely ridged plains material may be a less deformed or partially embayed form of tessera material. The age of densely ridged plains material relative to tessera is therefore unclear. Radar brightness for densely ridged plains material is similar to tessera material and generally brighter than other plains units (fig. 3*D*). However, this difference is probably mostly due to dense structural fabric rather than to inherent material properties.

Intratessera Plains Material

Many structural depressions within tessera material contain plains materials. Except where these plains are close to and have characteristics of regional plains, they are mapped as a separate unit, designated intratessera plains material (unit pi). This material is significantly darker than the adjacent tessera material and has radar brightness below the Muhleman curve (fig. 3*D*). Intratessera plains material fills in basins within tessera material and truncates tessera structures, indicating that it is clearly younger than tessera material. Because intratessera plains material is geographically isolated, its stratigraphic position relative to units other than tessera material is unknown. Therefore, it is shown in the correlation chart as being younger than tessera material, with uncertain upper and lower boundaries.

Ridged Plains Material

Ridged plains material (unit pr) is found within and near Eve, Carpo, and Tamfana Coronae and as inliers within plains in the north half of the map area. Similar to densely ridged plains material, structures are characteristic of the unit, but do not define it in all places. Radar brightness is similar to that of densely ridged plains material (fig. 3*D*). Ridged plains material truncates structures within tessera material, thus indicating that unit pr is older than unit t. Structures within the densely ridged plains and ridged plains materials are truncated at all boundaries with other plains units. Where the two units are in contact, ridged plains material truncates structures of the densely ridged plains material. Ridged plains material does not border tessera-adjacent textured plains material, so their age relationship cannot be determined. Ridged plains material touches edifice plains material, but their relative ages are also equivocal. Therefore, for plains materials exterior to tessera material, densely ridged plains material is the oldest. Ridged plains, edifice plains, and tessera-adjacent textured plains materials are younger than densely ridged plains material and older than all other plains materials, but the age relationship among these three units is not known. The general increase in the density and complexity of structural fabric with age in these plains materials suggests that regional tectonism waned with time.

Edifice Plains Material

Plains material associated with dense groupings of small, <4 km across edifices is exposed throughout the map area. Where stratigraphic relations are seen, this edifice plains material (unit pe) is commonly younger than tessera material and densely ridged plains material, but older than other adjacent plains units. Unit pe is at the boundaries of tessera material, within Tamfana Corona, and in a few areas surrounded by other plains units. The stratigraphic position of these outcrops and their location adjacent to tessera material, where topography is high, support the interpretation by Aubele (1996) and by Basilevsky and Head (1998) that some edifice plains material consists of small volcanic constructs largely buried by younger regional plains and flows and that, in general, the earliest plains may have been fed by dense groupings of small shields. However, within Eve Corona the edifice plains material appears relatively young, as it truncates corona structures. Similar, but less areally extensive, groupings of stratigraphically young edifices are found in other parts of the map area, but the scale of the geologic map prevents them from being depicted as a separate unit. These younger edifices may represent source regions for voluminous plains lavas that escaped burial, or they may represent more localized, volume-limited eruptions that formed contemporaneous with or after the plains units. Their presence is consistent with the interpretations of Addington (1999) and Guest and Stofan (1999) that shield fields are stratigraphically both older and younger than regional plains and that they therefore represent an ongoing geologic process. The relationships in the map area put the lower boundary of the edifice plains material at the top of the densely ridged plains material, with the upper boundary uncertain, as outlined below in the discussion of Eve Corona (see "Coronae" section), above the Carpo and Tamfana Corona flow material.

Tessera-Adjacent Textured Plains Material

The tessera-adjacent textured plains material (unit ptt) borders the southeastern margin of Alpha Regio, tessera inliers in the central part of the map area, and a steep-sided dome at 32.0° S., 10.5° E. (dome 105 of Pavri and others, 1992). The unit is characterized by a fine texture of ~ north-south-oriented radar-bright lineaments. The part of the unit adjacent to Alpha Regio slopes away from the tessera. In places (for example, 31.7° S., 7.5° E.) radar-dark fabric is continuous with radar-bright fabric in adjacent tessera material. All bordering plains and flow units truncate structures of this unit, indicating that they are younger. These observations suggest that tessera-adjacent textured plains material was an early plains unit that embayed the margins of tessera highlands before Stage 2 tessera-centered uplift (see "Geologic History" section below; Ivanov and Head, 1996). The lobe of tessera-adjacent textured plains material next to dome 105 is probably a kipuka.

Textured Regional Plains Material

The textured regional plains material (unit prt) is exposed in two large and several small patches south of Alpha Regio and Seoritsu Farra and as a patch in the southeastern part of the map area. The northern exposures are characterized by two predominant textures, a fabric of radar-bright lineaments that is generally oriented northwest-southeast and a surface that is mottled on a scale of 500 m or less. The southeastern exposure comprises a radar-bright region in the southwest and a brighter region in the northeast. Three sets of lineaments are apparent; they are oriented west-northwest to east-southeast, east-northeast to west-southwest, and north to south. Textured regional plains material is radar bright in contrast to adjacent plains units, but still plots below the Muhleman curve (fig. 3*D*). In the region 34° to −36° S., 11° to −14° E., the unit makes up the surface of a calderalike structure that is ~ 500 m above the surrounding regional homogeneous and digitate plains. Whether the outcrop is a partially buried caldera or is contiguous with and therefore part of unit prt is difficult to determine. However, because the outcrop gradually grades into the flat-lying portion of textured regional plains to the west and in many places has margins containing a fabric similar to that described above, the latter interpretation is favored. The adjacent lineated regional plains material truncates the structural fabric, indicating that unit prt is older. Fractures on the bordering tessera-adjacent textured plains material terminate where they meet textured regional plains material, indicating that they are probably older and have been filled with textured regional plains material. The patch of textured regional plains material in the southeastern part of the map area is adjacent to Ubastet Fluctus. Here, lineaments on the unit are truncated by the adjacent regional lineated plains material, indicating that unit prt is older.

Lineated Regional Plains Material

The most areally extensive unit in the map area is the lineated regional plains material (unit prl). Its northern sector is characterized by north-northeast-oriented grabens and lineaments extending from Fatua Corona (Brynhild Fossae) in V–32 quadrangle (about 1,500 km to the north) and east-west-trending wrinkle ridges. Brynhild Fossae, and thus the lineated plains unit, are truncated by the homogeneous regional plains material and by Ninhursag and Pachamama Coronae flow material along the southern boundary of the exposure (fig. 4), making the lineated regional plains material older. Radial structures from Eve, Carpo, Tamfana, and Selu Coronae, circumferential structures of Selu, and regional structures trending along the axis of the Alpha-Lada belt are superimposed on the lineated regional plains material, indicating that the unit formed during the evolution and development of the coronae and belt. The truncation of lineaments on the edifice plains (for example, 47° S., 11° E.), tessera-adjacent textured plains, and textured regional plains materials by the lineated regional plains material indicates that the lineated plains material is younger.

Radar-bright splotches, which are not mapped, are about 15 km across and occur individually and in dense clusters within the northern part of the map area, approximately between the craters Stuart and Zenobia. Single pits, ~ 0.5–1 km in diameter, in the center of many of these splotches suggest that they are low-relief shields.

Lineated regional plains material also is present in the southeast and south-central parts of the map area. At its boundary with the homogeneous regional plains material, ~100 km south of crater Deborah and south of the western arm of Vaidilute Rupes, lineaments and grabens have the same orientation as those of Brynhild Fossae in the north (fig. 5). The structures change orientation to ~north-south near Selu Corona and Tyche Tessera, where they are apparently strongly influenced by the two local coronae and extension belts (see below). Wrinkle ridges, with an ~east-west trend like that in the north, are also present. The similarity of some of these superposed structures is evidence that both the northern and southern parts of the lineated plains shared some structural deformation episodes. This similarity, together with the similar stratigraphic relationships with other units found in the two areas, argues that both provinces are the same unit. Small, isolated patches of plains in the southern part of the map area that lack these structures are mapped as lineated regional plains material because the radar brightness and textures are similar to those of larger regional lineated plains material patches and because they have equivalent stratigraphic positions. The lineated regional plains material is anomalously radar dark in halos distributed asymmetrically westward from Stuart and Zenobia. Outside of the halos, radar brightness varies from dark, such as near Selu Corona, to close to the Muhleman curve.

Homogeneous Regional Plains Material

The homogeneous regional plains material (unit prh) is the youngest regional plains unit. Except for portions of lineated regional plains affected by crater halos, it contains the darkest plains material in the map area. Its synthetic aperture radar (SAR) echo is generally 8 decibels or more below the Muhleman curve (fig. 3*D*). As the second youngest plains unit, it clearly truncates structures on the adjacent lineated regional plains material (see description above and figs. 4 and 5). The only plains unit that clearly truncates the homogeneous regional plains material is the digitate plains material. The homogeneous regional plains material generally resides within topographic lows on a scale ranging from tens of kilometers (for example, southwest of Stuart) to hundreds of kilometers. Its young age and its location strongly suggest that it formed from effusive volcanism in the waning stages of plains volcanism, when the gross topography was similar to that of today.

Digitate Plains Material

Digitate plains material (unit pd) comprises interlocking networks of digitate- to lobate-shaped radar-bright regions. The long axes of the digitate patterns generally radiate from a defined region, but not a recognizable source. Thus the digitate plains material is distinct from geographically isolated digitate flow units and flows associated with coronae and Sephira Mons. Like other plains units (except for edifice plains), the source vents apparently have been buried. The digitate plains material embays all other plains units where clear contact relations are seen and is therefore defined as the youngest plains unit in the map area. In most cases, structures present on adjacent plains units are covered by digitate plains material. One notable exception is seen where the ~north-south-oriented structures associated with Selu Corona (Yenkhoboy Fossae) and the Alpha-Lada belt cut the digitate plains material of Kaiwan Fluctus in Lavinia Planitia, indicating that the evolution of Selu and the belt continued after the deposition of this unit. Another exception shows wrinkle ridges both covered by and cutting the flows in Kaiwan Fluctus (see fig. 11), indicating that regional contractional strain overlapped in time with the prodigious volcanism that formed these plains.

VOLCANIC CONSTRUCT MATERIALS

Volcanic construct materials are divided among shield (unit vs), anemone (unit va), and dome (unit vd) materials. These units are categorized separately from plains and flow materials, as each mapped exposure composes a material that makes up an entire volcanic construct. In contrast, plains materials are extensive and may have some small constructs within them, and flow materials either have no recognizable source or are members of a sequence of flows on a large shield (for example, unit fSM_1 and unit fSM_2, as described below). In the former case, the small size of constructs on the plains prevents them from being mapped as separate units like those of the larger constructs discussed here. Instead, many of these small edifices are shown on the structure/volcano map (sheet 2). In the second case, volcanic construct materials are differentiated from flows on large shields because the former represents a style of volcanism that forms an individual edifice whereas the latter represents individual episodes within the history of a volcano.

Dome material comprises the steep-sided, commonly flat-topped structures found in the northwestern part of the map area. Domes greater than 15 km across are mapped as a separate unit. Owing to the scale at which features can be effectively shown on the geologic map (see Tanaka, 1994), smaller domes are indicated by structural symbols. The domes have radar brightness similar to that of the surrounding lineated regional plains (compare unit vd and unit prl in fig. 3), consistent with a more detailed SAR study by Ford (1994). In most cases the domes pre-date structural modification of these plains. For example, the fourth dome from the west in Seoritsu Farra contains a graben that, although confined to the dome, has the same orientation as grabens in the nearby plains, indicating that it formed in the same stress regime. The westernmost dome in Seoritsu Farra is crosscut by grabens that also cut the plains, clearly indicating that it pre-dates plains modification. However, this same graben is truncated by a heavily dissected dome to the southwest (29.87° S., 11.13° E.) (fig. 6). This relationship probably indicates that not all domes formed at the same time (Bridges and McGill, 1996), although some uncertainty exists because grabens can lengthen over time. A dome embayed by younger plains is present at 32.0° S., 10.5° E. (fig. 7). The dome's northern edge abuts a lobate, radar-bright surface that is interpreted as the same material as the tessera-adjacent textured plains. Structures on the dome and lobe are truncated by the adjacent, radar-dark, homogeneous regional plains material (unit prh). Thus, most domes predate plains structures and at least some (perhaps all) plains units. The easternmost three domes in Seoritsu Farra display subtle, radar-bright lineaments radiating from the edges of the domes into the surrounding plains (fig. 8). In some places, the lineaments are contiguous with radial lineaments on the surfaces of the domes, which suggests that either endogenous dome growth occurred after plains deposition or the domes loaded the rigid lithosphere, in both cases deforming the plains near the domes. Taking all of these observations together, the domes in the map area apparently formed before plains deposition, but at different times, with some possible activity after plains embayment.

Both shields and anemones are composed of digitate to lobate materials, which are presumably volcanic flows. The flows composing shield material are homogeneous and radially fan from a central mound or pit. Only two locales of shield construct materials, both north of the northwestern arm of Vaidilute Rupes (fig. 5), are mapped (Sephira Mons has two very extensive flow units that are mapped separately; see below). Anemone material is distinct from shield material in having radial flows with a more defined digitate character (fig. 5; Head and others, 1992). Both shield and anemone materials are commonly brighter than adjacent plains, although they plot below the Muhleman curve and are darker than many other plains units (fig. 3*E*). In places where only one plains unit is covered by these materials, the oldest buried unit is lineated regional plains material for anemone material and digitate plains material for shield material. Triple junctions with plains units, including the young homogeneous regional plains material, show that anemone and shield materials are always younger. These observations indicate that the earliest the shield and anemone materials could have formed was after the deposition of units pd and prl, respectively, whereas the latest stages, and perhaps all stages, of volcanic activity for these constructs post-dated the emplacement of all plains units.

FLOW MATERIALS

Flow materials are divided among isolated digitate and lobate flow material (unit fd) and flows associated with specific physiographic features. Digitate and lobate flow material generally has radar brightness higher than the adjacent plains or regional flow surface. This unit is distinct from digitate plains material, which comprises densely clustered flow assemblages. Where stratigraphic succession can be determined, digitate and lobate flow material is younger than the materials with which it is in contact (units pdr, ptt, prt, prl, prh, pd, fCT, and fNP). Digitate and lobate flow material is cut by, but does not fill, grabens south of Tamfana Corona. The grabens are probably associated with the regional Alpha-Lada extension belt. This age relationship indicates that coronae development continued after deposition of stratigraphically young flows.

Flows from eight physiographic features are distinct enough to map as separate units. The positions of prominent flow fronts are shown on the structure/volcano map (sheet 2). Many flows are geographically associated with coronae and are presumed to be genetically associated with them. Eve is the only corona within the map area that does not have distinct, areally extensive associated flows, although flows within Eve are present in the adjacent V–55 quadrangle (Ivanov and Head, 2001). Edifice plains material within Eve's interior in the map area could be related to its formation.

Ninhursag and Pachamama Coronae each have associated flow materials (units fN and fP, respectively). A regional unit near both coronae truncates lineaments on the individual coronae flows, indicating it is younger. This unit is geographically associated with both coronae and may therefore be related to their formation. It is referred to as Ninhursag and Pachamama Coronae flow material (unit fNP). This unit truncates structures on the regional lineated plains material to the north and east, indicating that late-stage volcanism from these small coronae post-dated deposition of this plains unit. It also borders homogeneous regional and digitate plains materials and member 1 of the unnamed shield flow materials, but the boundaries between unit fNP and these units are diffuse and age relationships cannot be determined with confidence. Some digitate and lobate flow material is on top of Ninhursag and Pachamama Coronae flow material. All of these age relationships are illustrated on the correlation chart by having unit fNP with diffuse boundaries above the level of unit prl and having units fN and fP with diffuse boundaries below the upper level of unit prl. The digitate and lobate flows are illustrated as being mostly younger than unit fNP.

The largest flow assemblage in the map area is within Ubastet Fluctus on and near Astkhik Planum. Unlike the flows in Kaiwan Fluctus, which are mapped as digitate plains material, the Ubastet flows emanate from the vicinity of Derceto Corona and are therefore considered a distinct material unit. Because of its association with Astkhik Planum, the unit is named Ubastet Fluctus and Astkhik Planum flow material (unit fUA). This unit is stratigraphically younger than each adjacent unit (t, b, pdr, prt, and prl,), except the flows from the unnamed shield (fSM_1 and fSM_2), where the age relations are equivocal. It is also younger than many structures that cut adjacent (and older) plains; for example, it covers the southeastern portion of Derceto Corona. The proximity of the corona to the source region of Ubastet Fluctus indicates a genetic association. The flows breach a gap in Vaidilute Rupes and have flow directions oriented downward along the regional slope. The flows near and to the east of the belt are larger, brighter, and more lobate than those west of the belt. The flows east of the belt are the brightest in the map area.

A large assemblage of flows is on the flanks and within the interior of Carpo and Tamfana Coronae (Carpo and Tamfana Coronae flow material, unit fCT). The Carpo and Tamfana Coronae flow material is younger than the lineated regional plains material (unit prl) but clearly older than some isolated digitate and lobate flows (unit fd) on top of the unit. It does not touch any other flow units. From these observations, Carpo and Tamfana Coronae flow material is placed on the correlation chart above the level of unit prl and contemporaneous with and older than some outcrops of unit fd (which has a large relative age range on the basis of stratigraphic relationships elsewhere in the map area, as discussed above).

An areally thin band of flows is on the southwest flank of Selu Corona and is designated Selu Corona flow material (unit fS). The lobate margins of these flows are oriented radially downslope from the interior of Selu, and the unit lies stratigraphically above the adjacent lineated regional plains material. Because it does not touch other flow materials, it is shown isolated on the correlation chart, higher than lineated regional plains material.

Sephira Mons (centered near 42.5° S., 28° E.) has proximal and distal flow units (member 2 [unit fSM_2] and member 1 [unit fSM_1], respectively, of Sephira Mons flow material). The units are mapped as flow materials as opposed to volcanic construct materials because the flows extend from the edifice onto the surrounding plains. The distal unit is areally extensive and in places it is difficult to distinguish it from adjacent plains and flows associated with Ubastet Fluctus. The proximal unit stratigraphically overlies the distal one and is therefore younger. Because of this, the distal flows may represent an early stage of effusive shield volcanism or they may pre-date the shield volcano. Digitate and lobate flows on the proximal unit have distinct outlines and do not appear to be truncated by the digitate plains material to the east, indicating that the latest stages of shield volcanism post-dates emplacement of the youngest plains materials. A tongue-shaped feature mapped as part of the distal member, adjacent to the east side of Vaidilute Rupes at ~41° S., 21° E., is very anomalous. It seems semi-transparent relative to the surrounding terrain; flow boundaries and textures that are distinct outside the tongue appear to maintain continuity but are less distinct inside (fig. 9). therefore, this feature could be a superficial deposit and not a flow.

MATERIALS OF IMPACT CRATERS

Impact crater materials are divided into interior, rim, and ejecta crater materials (unit ci) and crater flow material (unit cf). The floor is radar-dark and commonly contains a radar-bright central peak. The rim makes up an annulus partially to completely surrounding the floor. The ejecta are composed of assemblages of radar-bright hummocks outside the rim, commonly distributed radially.

The crater outflow comprises radar-bright digitate to lobate materials, interpreted as impact melt (Asimow and Wood, 1992; Schaber and others, 1992), and is referred to as crater flow material (unit cf). The unit is generally external to and distributed radially from the crater. The major exception is the crater Stuart, whose rim, wall, and floor are interpreted as being completely covered with radar-bright impact melt. The emissivity of the crater flow material in Stuart is 0.73. This value is in marked contrast to materials in the rest of the map area, which have emissivity values of 0.80–0.92 (fig. 10). The radar brightness of crater outflow material is 2 decibels or more above the Muhleman curve (fig. 3*A*).

Of the fifteen craters in the map area, two are embayed by plains lavas. Bernice (40.7° S., 14.8° E.) is filled with digitate plains material, therefore it is clearly older. Dorothy (35.4° S., 11.3° E.) is embayed by homogeneous regional plains material and, in turn, has ejecta deposited on top of lineated regional plains material, indicating that it formed sometime between the emplacement of the two plains units. All the other craters are clearly younger than adjacent units. Some crater materials truncate structures, establishing relative ages. For example, outflow and ejecta from Stuart (30.8° S., 20.2° E.) and Sophia (28.6° S., 18.8° E.) fill grabens (Brynhild Fossae) associated with Fatua Corona (within V–32 quadrangle). Therefore, the age sequence is emplacement of lineated plains, followed by regional extension from Fatua, and terminating with the impacts of Stuart and Sophia. Muriel (41.7° S., 12.4° E.) outflow material fills both a graben that radially emanates from Selu Corona and a north-south-oriented graben possibly associated with Fatua. Therefore, Muriel post-dates extensional strains from Selu and possibly Fatua. A radial graben south of Selu Corona (Yenkhoboy Fossae) post-dates the digitate plains of Kaiwan Fluctus. If all of Selu's radial grabens are the same age, then Muriel must postdate the digitate plains as well. Individual crater ages are shown on the correlation chart.

SURFICIAL MATERIALS

Halos with diffuse boundaries superimposed on plains materials are associated with the craters Stuart and Zenobia (fig. 2). Both halos are distributed asymmetrically westward from the craters, supporting the interpretation that they are composed of materials thrown into the atmosphere by meteorite impact and then re-distributed by westward winds at ~50 km altitude (Arvidson and others, 1992). Stuart's halo is particularly large, with a maximum north-south dimension of 1,500 km. The halos are very radar dark, about 8 dB below the Muhleman curve (fig. 3*D*).

Wispy tendrils and splotches of radar-dark and radar-bright materials are present throughout the map area. In many places, these are not clearly associated with flows or structures, strongly suggesting that they are surficial. They are probably the result of eolian re-distribution of fine-grained material (Greeley and others, 1992).

STRUCTURAL GEOLOGY

The structures in the map area are diverse and range in size from over 1,000 km down to the limit of resolution (~100 m). This section describes major structural features and classes of structures. Many structures discussed are illustrated on the geologic map (sheet 1). A more detailed representation of structures is shown on the structure/volcano map (sheet 2).

EXTENSIONAL BELTS

The map area contains the Alpha-Lada and Decerto-Quetzalpetlatl extensional belts (Baer and others, 1994). Both structures are characterized by corona chains (individual coronae are described below) and interconnecting sets of approximately parallel lineaments and grabens. The two belts intersect at Astkhik Planum. Alpha-Lada trends north-northwest, is 50–200 km wide, and stretches over 6,000 km from Eve Corona in the north to an unnamed corona in V–56 quadrangle to the south. As noted by Baer and others (1994), the relationship between coronae and belt structures is complex. In some cases, regionally trending grabens of the belt crosscut coronae, such as at Tamfana and at Eve. In contrast, radial grabens from Selu both cut and are truncated by the regional grabens and to the east-southeast are deflected along the trend of the belt. Grabens associated with Alpha-Lada cut stratigraphically young flows of digitate plains material in Kaiwan Fluctus, indicating that evolution of the belt continued into the final stages of deformation within the map area.

The Decerto-Quetzalpetlatl extensional belt trends north-northeast, is as much as 300 km wide or more, and extends approximately 2,000 km from the south margin of the Astkhik Planum to Quetzalpetlatl Corona in V–56 quadrangle. Only a small part of its northern portion is within the map area. Here, its trend is defined by generally north-northeast-trending grabens and lineaments south of Selu Corona (Yenkhoboy Fossae) and west of Astkhik Planum. Near Selu, the belt structures and lineaments are deflected parallel to the trend of the Alpha-Lada belt, indicating that the stress field of Alpha-Lada was in place when the Decerto-Quetzalpetlatl belt formed. This relationship strongly suggests that formation of the two extensional belts overlapped in time (Baer and others, 1994).

CORONAE

Of the seven coronae in the map area, five of them—Eve, Carpo, Tamfana, Selu, and Derceto—are within the more broadly defined Alpha-Lada extensional belt (Baer and others, 1994). As discussed above, superposition relations among structures indicate that development of Alpha-Lada and the coronae overlapped in time. These five coronae are described below, followed by Pachamama, Ninhursag, and structures associated with Fatua.

Eve Corona (32.0° S., 359.8° E.) is approximately circular and about 400 km in diameter. Its interior is covered by plains materials and its exterior is marked by annular ridges and radial grabens. The radial structures generally pre-date concentric lineaments of the annulus, suggesting that Eve, like other coronae with similar structural relationships, formed by a process of doming followed by central subsidence (Squyres and others, 1992a; Stofan and others, 1992). The interior of Eve contains some radar-bright lava flows and shields. Most structures on the ridged plains material associated with Eve do not appear to cut tessera material. However, these structures are judged as younger than tessera material because (1) tessera structures stop at the boundary between the tessera and ridged plains materials here and elsewhere (see discussion of tessera material above), (2) tessera material in this area crops out as elevated blocks, where strain likely was accommodated differently than in the plains, and (3) a few structures actually do cross tessera material. The most heavily tectonized portions of Eve are within the densely ridged plains material. A lower density of structures is within the ridged plains and Carpo and Tamfana Coronae flow materials (in the latter case, many of the regional north-northwest-trending structures are actually associated with the Alpha-Lada belt). Therefore, Eve Corona formation began after the deposition of densely ridged plains material, continued at a slower pace after the deposition of the ridged plains and Carpo and Tamfana Coronae flow materials, and terminated before deposition of relatively young edifice plains material.

Carpo Corona (37.5° S., 3.0° E.) is ~200 km wide and predominately made up of a dense array of radial ridges, grabens, and lineaments. These structures and lineaments are especially concentrated on the eastern and western sides of Carpo. The density of structures is greater than that of any other corona in the map area, making determination of relative ages difficult. Carpo structures cut densely ridged plains material and younger units, including, in some places, digitate and lobate flow material. On the correlation chart, this relation puts the beginning of Carpo evolution at the base of densely ridged plains material, with the end uncertain.

Tamfana Corona (36.3° S., 6.0° E.) is about 300 km across. Its shape, as defined by annular ridges, is approximately circular. A major exception is at the eastern margin, where annular structures abruptly change orientation from north-northeast to northwest. The interior of Tamfana is filled with radar-bright lava flows and shields. Tamfana structures are pervasive within the densely ridged plains material. They also are present, but at a lower density, within lineated regional plains and Carpo and Tamfana flow materials. They are truncated by edifice plains material. In the correlation chart, these relationships put the evolution of Tamfana Corona beginning at the base of the densely ridged plains material. Because the edifice plains material have an uncertain upper boundary, the ending of Tamfana Corona evolution cannot be well constrained and is shown as open on the correlation chart.

Selu Corona (42.5° S., 6.0° E.) is about 300 km in diameter and contains prominent radial and concentric structures. Elongated basins are present in the western and southwestern parts of the corona. They are both truncated and crosscut by concentric structures. These concentric structures are within two annuli that, except for areas in the northeast, completely encircle the corona center. Lobate flows radiate from the east half of the outer annulus. Structures associated with Selu cut densely ridged plains material in the interior of the corona, with radial outlying structures cutting materials ranging in age from tessera to digitate plains. On the correlation chart, this puts the base of Selu Corona at the bottom of the densely ridged plains material, with the upper boundary uncertain.

Derceto Corona (46.8° S., 20.2° E.) is about 100 km by 200 km, with its long axis oriented northwest-southeast. Circumferential lineaments and grabens encircle its outer edge. These structures become partially or completely covered by Ubastet Fluctus and Astkhik Planum flow material in the southeast. An ~30-km-wide moat within the northwestern interior of the corona is surrounded by concentric annuli. Subradial lineaments within the innermost concentric annuli terminate ~3 km from the moat's center. Outside the moat, radial lineaments are absent, indicating that these structures either never formed or were buried by subsequent lava flows or surficial deposits. Although flows within Ubastet Fluctus do not radiate from Derceto itself, they do emanate from near the corona, suggesting a genetic relationship. Ubastet Fluctus embays adjacent regional plains and is therefore relatively young, which strongly suggests that Derceto is also young and that it post-dates most other coronae structures in the Alpha-Lada belt.

Ninhursag (38.0° S., 23.5° E.) is an ~125-km-wide corona with radial and concentric lineaments and grabens. The concentric structures are contained within two annuli. The outer margins of the western radial lineaments and grabens are deflected somewhat to the south. All of the structures cut flows clearly associated with Ninhursag. Flows distributed over a broader region distal from both Ninhursag and Pachamama Coronae (36.0° S., 21.8° E.), mapped as Ninhursag and Pachamama Coronae flow material, surround Ninhursag and truncate many of its radial structures. Thus, the more regional flows associated with the two coronae are younger than those central to Ninhursag.

Pachamama is designated as a corona by the International Astronomical Union (1999), although it is not recorded in the catalog of Stofan and others (1992). Grabens and lineaments radiate from a circumferential zone ~75 km by 125 km. The elongated pattern of these structures makes it somewhat similar to oval-shaped Derceto Corona to the southwest. Concentric structures are rare, although one prominent semi-concentric annular scarp that drops radially away from the corona is present in the south. Both the interior and outer margins of Pachamama are filled with flows associated with both it and Ninhursag Corona (Ninhursag and Pachamama Coronae flow material).

Fatua Corona, although within V–32 quadrangle, has many radial grabens and lineaments that extend up to 1,500 km away from it into V–44 quadrangle. In the northern part of the map area these are named Brynhild Fossae. The structures, oriented north-northeast, crosscut the lineated and textured regional plains and portions of the homogeneous regional plains. Similar orientations of lineaments and grabens south of the western arm of Vaidilute Rupes suggest that they are also associated with Fatua and have been covered to the north by digitate and homogeneous regional plains. However, structural relationships in this region are complex and any stresses from Fatua have been strongly influenced by the two extensional belts and Vaidilute Rupes.

PLAINS STRUCTURES

Wrinkle Ridges

Wrinkle ridges are present almost exclusively within the northern and southern areas of lineated regional plains material and in digitate plains material of Kaiwan Fluctus in Lavinia Planitia. A few are within the Carpo and Tamfana Coronae flow material. Except for some isolated cases, all wrinkle ridges are oriented approximately east-west. They average 30 km long and 2 km wide. The absence of wrinkle ridges in the midlatitudes of the map area, including areas composed of relatively old (pre-digitate) plains materials, may be due to the complex assemblage of structures in this region absorbing strain along preexisting faults. The timing of the northern wrinkle ridges can only be constrained to be after the formation of the regional lineated plains material. The wrinkle ridges on the digitate plains material of Kaiwan Fluctus both pre-date and post-date flows, indicating that the southern set of ridges formed over a long time interval after deposition of the lineated regional plains material (fig. 11).

Other Plains Structures

Other structures confined to the plains include grabens, ridges, fractures, and lineaments. Unlike the wrinkle ridges, the orientations of these features vary considerably. In some cases they are restricted to individual units, such as the densely ridged plains material, whereas in other examples structures cut across unit boundaries (for example, subtle northwest-trending fabric between the digitate plains material and tessera-adjacent textured plains material at ~31° S., 11° E.). Some structures are linear whereas others curve along their length, much like corona structures.

ASTKHIK PLANUM AND ASSOCIATED STRUCTURES

Astkhik Planum has dimensions of ~1,600 km by 600 km and is elevated a few hundred meters above the surrounding plains (Baer and others, 1994). The Ubastet Fluctus and Astkhik Planum flow material contains radar-bright digitate fingers that project downslope from the plateau, bisecting Vaidilute Rupes (47° S., 27° E.), thus indicating that the plateau is older than this flow unit. No age relations with other units are obvious.

The eastern and northern margins of Astkhik Planum are bounded by Vaidilute Rupes. The troughs and ridges of this belt slope away from the plateau. The eastern edge of the northeastern segment of Vaidilute Rupes is within an ~600-m-deep trough. This topography is similar to that at Artemis and Eithinoha Coronae, where lithospheric subduction has been suggested (Sandwell and Schubert, 1992a,b). The translucent nature of a tonguelike feature to the east of Vaidilute is suggestive of a superficial deposit (fig. 9). Residing within the trough, the tongue may be material slumped off the edge of the belt. To the north, the belt splits into two segments, one trending east-west and the other northwest-southeast. The projection of the strike of the northwest-southeast-trending segment into the plains intersects the upper part of the ovoidal, calderalike structure within the textured regional plains material (see discussion above). Like Vaidilute Rupes, this structure is elevated above the plains. It is therefore possible that Vaidilute Rupes and the structure are related.

The western and southwestern boundary of Astkhik Planum in the map area is bordered by a 0.5- to 1-km-deep trough (part of which is in Hanghepiwi Chasma). The edges of the southwestern part of the trough are bounded by lineaments and by down-dropped blocks that trend in the same direction as the trough's long axis. Structural fabric to the southwest of the trough has a similar appearance to that found to the northeast. The fabric terminates at the trough walls. These observations indicate that the trough is a rift valley filled with plains lavas. To the north, the trough ceases continuity and is replaced by elongate basins at the southern margin of Tyche Tessera. The plateau boundary, as defined by a prominent topographic discontinuity (fig. 1), then wraps around the edge of Selu Corona and, trending east, merges with the east-west arm of Vaidilute Rupes. South of V–44 quadrangle, in V–56 quadrangle, the trough trends south and then east, being composed of tessera material at its southernmost, east-west-trending boundary. At the eastern edge of this region, the trough merges with Vaidilute Rupes, indicating that both structures are related to the formation of Astkhik Planum.

TESSERA

Alpha Regio

The structural geology within the tessera material is complex, exhibiting several different structures oriented along various trends. Alpha Regio, the largest tessera region in the map area, displays troughs, ridges, and lineaments or fractures. The troughs, commonly classified as "ribbons" (Hansen and Willis, 1996), are steep-sided, shallow, and up to 3 km wide. They generally trend northwest-southeast, but in places exhibit different orientations. The ridges are ~5–10 km wide and spaced ~15–25 km apart. They generally trend north-east-southwest, but in places curve along their crest, forming s-shaped, u-shaped, and snakelike patterns. On the basis of their morphology, they are interpreted as folds. In the southeastern portion of Alpha Regio, the orientations of many ridges are parallel to the boundary between tessera material and adjacent plains materials. The ridges and their associated intervening basins are classified as "basin-and-dome terrain" by Hansen and Willis (1996). The basins are, in most cases, more radar-dark than the ridges. Radar-bright lineaments at the limit of resolution and distribution along trends distinct from the ridges and ribbons are common. Where ribbons and ridges are generally absent, such as portions of southeastern Alpha Regio, the lineaments define the major tessera fabric.

Determining an age sequence among the structural fabrics is difficult, although Hansen and Willis (1996) argue that ribbons pre-date the basin and dome patterns whereas Gilmore and others (1998) contend the opposite is true. In some places, determining whether the basin floors represent the original depression of a folded surface or later flows that filled in the depression is not possible, as many ribbons cease continuity where they border basin floors, but others do not. Despite these complexities, overprinting of structural fabrics clearly indicates that Alpha Regio underwent several phases of structural deformation (Bindschadler and others, 1992; Hansen and Willis, 1996).

Tyche Tessera

Tyche Tessera is the second largest tessera region in the map area, being approximately 15 km by 80 km, with its long dimension oriented northwest-southeast. The structural fabric within Tyche is more unidirectional than most tessera material, with a strong northwest-southeast orientation dominating over more subtle fabrics oriented north-northwest to south-southeast, north-south, and northwest-southeast. Several elongate basins with radar-dark floors are present. These include long, ~ 3-km-wide, grabenlike depressions that appear to be radial fractures associated with Selu Corona. As such, they are unrelated to stress events that caused most of the Tyche Tessera structures. Dense lineaments at the limit of FMAP resolution are the dominant structures.

Inliers

Several tessera inliers are present in the map area. Most have elongate to arclike forms, with length-to-width ratios of 10:1 or more. These long inliers generally display ridges, interpreted as folds, and intervening troughs that strike along trends similar to the inliers' long axes. Grabens and lineaments oriented nearly perpendicular to each other are common. Some inliers are more equant in shape and display varying structural styles, ranging from dense packages of radar-bright lineaments at the limit of resolution (32° S., 14° E.) to small-scale lineaments grouped with larger scale grabens (37° S., 17.5° E.) to fabrics dominated by ridges and intervening basins (Clidna Tessera; 42° S., 29° E.). Penetration of plains structures is more apparent within inliers than it is for larger tessera blocks. Adjacent inliers commonly share structural trends and styles.

VOLCANIC FEATURES

Sephira Mons is the only large shield volcano within the map area (42.5° S., 28° E.). It is about 150 km wide and has two associated flow units, as described in the stratigraphy section above.

A possible flooded caldera is present at 35.5° S., 13° E. Smaller edifices are abundant in the map area. With sizes down to the limit of resolution, they number in the hundreds or even thousands. Many are grouped in clusters that appear to be associated with adjacent flows.

The map area contains nine steep-sided domes larger than 15 km in diameter (unit vd). These domes are significant, as they probably are the manifestation of viscous, silicic lava (Pavri and others, 1992; Ivanov and Head, 1999), a rarity on Venus, or of basaltic lava emplaced under constrained eruption conditions (Bridges, 1995, 1997; Stofan and others, 2000). All of these domes are within 200 km of Alpha Regio (discussed in detail in the stratigraphy section). Smaller steep-sided domes also are present, mostly within the northwestern part of the map area. Many of the small steep-sided domes and shields contain one or more pits on their flanks. Because of the scale at which small outcrops can be effectively represented on the geologic map (sheet 1), the small domes and other volcanic features are shown on the structure/volcano map (sheet 2).

The northern segment of Kallistos Vallis, a compound channel more than 1,200 km long, is present in the south-central region of the map area (47.5° S. and southward, 19°-20° E.). The ~250-km segment within the map area consists of a northern collapse pit, south of which is a deep trough. The trough in this region appears structurally controlled, consisting of straight segments that parallel the structural grain along the margin of Astkhik Planum. In V–56 quadrangle these segments become anastomosing channels with intervening streamlined islands that, in turn, merge into a distributary lava flow system (Parker and others, 1991; Baker and others, 1992, 1997). The northernmost distal branches of the Kallistos channel system appear to have fed flows that ponded in a trough west of and straddling the southern arm of Vaidilute Rupes in the map area. Some of the lavas that flowed eastward and downslope from the Astkhik Planum across the gap between the northern and southern arms of Vaidilute may be an extension of Kallistos flows. However, determining whether the ultimate source of the flows is Kallistos' vents or the Ubastet Fluctus vents associated with Derceto Corona is difficult.

GEOLOGIC HISTORY

As with most (or all) of Venus, the geology within this map area is complex. Nevertheless, a general geologic history can be derived from the key stratigraphic and structural relationships presented above. Here, these observations are used to present an overall geologic history of Kaiwan Fluctus quadrangle. This history is divided into three stages, the first characterized by significant structural development and deformation, the second by coronae formation and plains emplacement, and the last by localized volcanism and small coronae and wrinkle ridge development.

Stage 1: Formation of tessera and belt materials and Astkhik Planum—The earliest phases of evolution of the map area were characterized by development of tessera and belt materials and the formation of Astkhik Planum. The belt materials and Astkhik Planum formed contemporaneously but their age relative to tessera is unknown. Tessera formation initially consisted of strong polyphase deformation, followed by plains embayment at tessera margins and uplift. The times of formation of various tessera blocks relative to one another cannot be established, but all pre-date major plains emplacement. Volcanism forming plains within tessera blocks occurred during and after deformation. Structural development of tessera and uplift continued into later stages, but at a progressively less intense pace.

Stage 2: Formation of steep-sided domes, regional plains, and coronae in the Alpha-Lada extensional belt—Steep-sided domes generally formed before plains deposition, after which some domes continued to grow endogenously. This dome growth was followed by the successive deposition of plains materials (except the digitate plains material, which is assigned to stage 3). Groups of small edifices (mainly shields) deposited lavas on some of the early plains, but later plains formed by voluminous, high effusion rate eruptions. Regional tectonism waned over time, with the oldest plains preserving a longer record of structural deformation than younger plains. Regional uplift centered on tessera material declined with time, such that older plains adjacent to tessera were protected from embayment by later, younger plains. Low effusion rate volcanism formed clusters of small edifices on the surfaces of the plains in certain areas.

Formation and most of the geologic evolution of Eve, Carpo, Tamfana, and Selu Coronae and the regional north-northwest-trending lineaments and grabens of the Alpha-Lada belt were coincident with plains deposition. Radial structures from Fatua Corona (in V–32 quadrangle) also formed during this time. Some coronae and belt activity continued into stage 3. Some wrinkle ridge development may have occurred in the northern part of the map area during this stage.

Stage 3: Production of digitate flow fields, small coronae, centralized volcanic sources, and wrinkle ridges—Despite waning tectonism, volcanism continued into the latest stages of the evolution of the map area. Large-scale digitate flow fields were emplaced through voluminous, high effusion rate eruptions. Regional north-south contractional strain deformed plains into east-west-trending wrinkle ridges before, during, and after deposition of these flow fields. One of the fields, Ubastet Fluctus, formed contemporaneously with Derceto Corona, one of three small coronae in the map area. The other two coronae, Pachamama and Ninhursag, and their associated flows also formed during this period. Waning structural deformation associated with the Alpha-Lada belt continued after the emplacement of Kaiwan Fluctus. The final volcanic episodes in the map area were the formation of Sephira Mons and smaller shields and anemones.

DISCUSSION

On the basis of impact crater counts, the surface of Venus is estimated to be 300–800 million years old (Phillips and others, 1992; Schaber and others, 1992; McKinnon and others, 1997). The apparent random distribution of craters and the relative absence of embayed or tectonized craters on the regional plains suggest that most geologic activity was confined to a short interval following a period of extensive resurfacing (Head and others, 1992; Schaber and others, 1992), although other interpretations of the cratering record have questioned this model (Hauck and others, 1998). The geology within the Kaiwan Fluctus quadrangle is consistent with this model and indicates that tectonic and volcanic activity was most intense early in the preserved history, with both processes waning in intensity over time. This observation is one that has been made for much of Venus (Head and others, 1992; Schaber and others, 1992). Some of the most important contributions of this map are not the support of this general idea, but rather the details the stratigraphic relationships and structures reveal.

The most tectonized regions of the map area, the tessera and belt materials, are also the oldest stratigraphically. In the case of tessera material, these old ages are in agreement with several other studies (Ivanov and Basilevsky, 1993; Gilmore and others, 1997; Basilevsky and Head, 1998), whereas age estimates for belts relative to adjacent plains are variable (Squyres and others, 1992b; Rosenberg, 1995). Where age relations can be determined, tessera and belt materials are older than surrounding plains in the map area, indicating that the earliest preserved history was one marked by intense strain that deformed pre-existing materials. In the case of tessera material, multiply oriented, superposed structures indicate that this deformation was polyphase, occurring over some interval or divided among several episodes before plains embayment. In contrast, the structures within the Vaidilute Rupes scarp belt are oriented predominantly along the strike of the belt, indicating unidirectional compression associated with the uplift and extension of Astkhik Planum.

Regional-scale uplift appears to have occurred early in the history of the region, uplifting Astkhik Planum as well as Alpha Regio and some tessera inliers. The preservation of plains-embayed tessera margins at these tesserae that dip from the tessera boundaries toward the plains indicate that the later parts of some tessera evolution were characterized by waning uplift and tectonization, consistent with observations of tessera material elsewhere on Venus (Ivanov and Head, 1996; Gilmore and others, 1997).

The subsequent tectonic and volcanic style in the map area changes with stratigraphic age. Tectonism wanes and, in most cases, becomes more localized. The oldest plains generally contain the most structures, as illustrated by the dense arrays of lineaments on the stratigraphically old densely ridged and ridged plains units and the relative absence of these features on the stratigraphically young regional homogeneous and digitate plains materials. The main exceptions to this observation are the wrinkle ridges, which formed after deposition of the younger plains units, in some cases post-dating digitate plains.

The evolution of tectonic style is also manifested in changes of coronae characteristics with age. The oldest coronae in the map area—Eve, Carpo, Tamfana, and Selu—have both radial and concentric structures, with the radial structures generally being older than the concentric ones. In contrast, the younger coronae—Ninhursag and especially Pachamama—are dominated by radial lineaments. This tectonic style is broadly consistent with the classic hypothesis for coronae formation, in which mantle diapirs impinge against a relatively thin venusian lithosphere shortly after global resurfacing (Janes and others, 1992; Squyres and others, 1992a; Stofan and others, 1992; Janes and Squyres, 1993). The resulting thermal and dynamic support uplifts topography, causing radial fracturing and volcanism. Eventually plume strength wanes, causing subsidence and the formation of concentric fractures. The mapping relations in V–44 quadrangle suggest that subsidence occurred for the early coronae, but a thicker and more rigid lithosphere inhibited this subsidence for the younger coronae. The old coronae are also much larger than the young coronae, which suggests that the putative early, thin lithosphere was more broadly affected by diapiric stresses than the later, thicker lithosphere. A major exception to this hypothesis is Derceto Corona, which seems relatively young, yet has no radial lineaments. Additional exceptions to the original corona model have been documented elsewhere on Venus (Copp and others, 1998). Therefore, the ideas on corona evolution presented here should be considered as hypotheses that can be tested elsewhere on the planet.

Many aspects of volcanism also change with age. The steep-sided domes in almost all cases appear to be relatively old, similar to observations of other domes on Venus (Bridges and McGill, 1996; Ivanov and Head, 1999). This age relationship indicates that the process responsible for dome formation waned with time as the lithosphere thickened. Much (but not all) of the edifice plains material is also relatively old and, like the domes, is embayed by adjacent plains units. Therefore, the earliest preserved evidence for volcanism is that of a localized, low effusion rate style. This style gives way to more voluminous, probably high effusion rate, volcanism that deposited the regional plains materials. Although this was the predominant mode, small flows and edifices within many regional plains materials indicate that more localized eruptions with relatively low effusion rates also occurred. The latest phases of activity are recorded by digitate flows and volcanism from Sephira Mons. The digitate flows, like plains in general, are probably indicative of high effusion rate volcanism (Magee Roberts and others, 1992). The young age of the shield volcano indicates that the lithosphere was of sufficient strength and thickness to support the construct when it formed, in agreement with other studies (McGill, 1994; Solomon and others, 1994; McGovern, 1996). This young age also is consistent with young shield ages derived from crater abundance statistics (Namiki and Solomon, 1994; Price and others, 1996).

In summary, the model for venusian geologic history of planetary cooling and lithospheric thickening following an initial resurfacing event is generally supported by the mapping relations. A competing scenario whereby geologic activity in the map area has been proceeding at a constant rate since the deposition of the stratigraphically oldest units seems unlikely given that only 2 of the 15 craters in the map area are embayed by plains lavas and that the tectonization of tessera craters, although present, is minor. The earliest geologic phases were dominated by intense, broad-scale tectonic activity that included compression, extension, and regional uplift, whereas the later phases were dominated by volcanic processes. Most geologic activity on the surface occurred over a brief interval of time, although some activity has declined more slowly and may still be occurring today.

REFERENCES CITED

Addington, E.A., 1999, Clusters of small volcanoes on Venus, *in* Lunar and Planetary Science Conference XXX: Houston, Lunar and Planetary Institute, abstract 1281 [CD-ROM].

Arvidson, R.E., Greeley, G., Malin, M.C., Saunders, R.S., Izenberg, N., Plaut, J.J., Stofan, E.R., and Shepard, M.K., 1992, Surface modification of Venus as inferred from Magellan observations of plains: Journal of Geophysical Research, v. 97, no. E8, p. 13,303–13,318.

Asimow, P.D., and Wood, J.A., 1992, Fluid outflows from Venus impact craters—Analysis from Magellan data: Journal of Geophysical Research, v. 97, no. E8, p. 13,643–13,666.

Aubele, J.C., 1996, Akkruva small shield plains—Definition of a significant regional plains unit of Venus [abs.], *in* Lunar and Planetary Science Conference XXVII: Houston, Lunar and Planetary Institute, p. 49–50.

Baer, G., Schubert, G., Bindschadler, D.L., and Stofan, E.R., 1994, Spatial and temporal relations between coronae and extensional belts, northern Lada Terra, Venus: Journal of Geophysical Research, v. 99, no. E4, p. 8355–8369.

Baker, V.R., Komatsu, G., Parker, T.J., Gulick, V.C., Kargel, J.S., and Lewis, J.S., 1992, Channels and valleys on Venus—Characteristics, geologic setting, and eruption conditions from Magellan data: Journal of Geophysical Research, v. 97, no. E8, p. 13,421–13,444.

Baker, V.R., Komatsu, G., Gulick, V.C., and Parker, T.J., 1997, Channels and valleys, *in* Bougher, S.W., Hunten, D.M., and Phillips, R.J. (eds.), Venus II: Tucson, University of Arizona Press, p. 757–793.

Basilevsky, A.T., and Head, J.W., 1998, The geologic history of Venus—A stratigraphic view: Journal of Geophysical Research, v. 103, no. E4, p. 8531–8544.

Bindschadler, D.L., deCharon, A., Beratan, K.K., Smrekar, S.E., and Head, J.W., 1992, Magellan observations of Alpha Regio—Implications for formation of complex ridged terrains on Venus: Journal of Geophysical Research, v. 97, no. E8, p. 13,563–13,578.

Bridges, N.T., 1995, Submarine analogs to venusian pancake domes: Geophysical Research Letters, v. 22, no. 20, p. 2781–2784.

———1997, Ambient effects on basalt and rhyolite lavas under venusian, subaerial, and subaqueous conditions: Journal of Geophysical Research, v. 102, no. E4, p. 9243–9255.

Bridges, N.T., and McGill, G.E., 1996, Formation and modification ages of some steep-sided domes on Venus (abs.), *in* Lunar and Planetary Science Conference XXVII: Houston, Lunar and Planetary Institute, p. 165–166.

Campbell, B.A., 1995, Use and presentation of Magellan quantitative data in Venus mapping: U.S. Geological Survey Open-File Report 95–519, 32 p.

Copp, D.L., Guest, J.E., and Stofan, E.R., 1998, New insights into coronae evolution—Mapping on Venus: Journal of Geophysical Research, v. 103, no. E8, p. 19,401–19,417.

Ford, P.G., 1994, Radar scattering properties of steep-sided domes on Venus: Icarus, v. 112, no. 1, p. 204–218.

Gilmore, M.S., Ivanov, M.A., Head, J.W., and Basilevsky, A.T., 1997, Duration of tessera deformation on Venus: Journal of Geophysical Research, v. 102, no. E6, p. 13,357–13,368.

Gilmore, M.S., Collins, G.C., Ivanov, M.A., Marinangeli, L., and Head, J.W., 1998, Style and sequence of extensional structures in tessera terrain, Venus: Journal of Geophysical Research, v. 103, no. E7, p. 16,813–16,840.

Greeley, R., Arvidson, R.E., Elachi, C., Geringer, M.A., Plaut, J.J., Saunders, R.S., Schubert, G., Stofan, E.R., Thouvenot, E.J.P., Wall, S.D., and Weitz, C.M., 1992: Aeolian features on Venus—Preliminary Magellan results: Journal of Geophysical Research, v. 97, no. E8, p. 13,319–13,346.

Guest, J.E., and Stofan, E.R., 1999, A new view of the stratigraphic history of Venus: Icarus, v. 139, no. 1, p. 55–66.

Hansen, V.L., and Willis, J.J., 1996, Structural analysis of a sampling of tesserae—Implications for Venus geodynamics: Icarus, v. 123, no. 2, p. 296–312.

Hauck, S.A., Phillips, R.J., and Price, M.H., 1998, Venus—Crater distribution and plains resurfacing models: Journal of Geophysical Research, v. 103, no. E6, p. 13,635–13,642.

Head, J.W., Crumpler, L.S., Aubele, J.C., Guest, J.E., and Saunders, R.S., 1992, Venus volcanism—Classification of volcanic features and structures, associations, and global distribution from Magellan data: Journal of Geophysical Research, v. 97, no. E8, p. 13,153–13,197.

Herrick, R.R., Sharpton, V.L., Malin, M.C., Lyons, S.N., and Feely, K., 1997, Morphology and morphometry of impact craters, *in* Bougher, S.W., Hunten, D.M., and Phillips, R.J. (eds.), Venus II: Tucson, University of Arizona Press, p. 1015–1046.

International Astronomical Union, 1999, Working Group for Planetary System Nomenclature, *in* Proceedings of the 23d General Assembly, Kyoto, 1997: Transactions of the International Astronomical Union, v. 23B, p. 236–251.

Ivanov, M.A., and Basilevsky, A.T., 1993, Density and morphology of impact craters on tessera terrain, Venus: Geophysical Research Letters, v. 20, no. 23, p. 2579–2582.

Ivanov, M.A., and Head, J.W., 1996, Tessera terrain on Venus—A survey of the global distribution, characteristics, and relation to surrounding units from Magellan data: Journal of Geophysical Research, v. 101, no. E6, p. 14,861–14,908.

———1999, Stratigraphic and geographic distribution of steep-sided domes on Venus—Preliminary results from regional geological mapping and implications for their origin: Journal of Geophysical Research, v. 104, no. E8, p. 18,907–18,924.

———2001, Geologic map of the Lavinia Planitia Quadrangle (V–55), Venus: U.S. Geological Survey Geologic Investigations Series I–2684, scale 1:5,000,000.

Janes, D.M., and Squyres, S.W., 1993, Radially fractured domes–A comparison of Venus and Earth: Geophysical Research Letters, v. 20, no. 24, p. 2961–2964.

Janes, D.M., Squyres, S.W., Bindschadler, D.L., Baer, G., Schubert, G., Sharpton, V.L., and Stofan, E.R., 1992, Geophysical models for the formation and evolution of coronae on Venus: Journal of Geophysical Research, v. 97, no. E10, p. 16,055–16,067.

Magee Roberts, K., Guest, J.E., Head, J.W., and Lancaster, M.G., 1992, Mylitta Fluctus, Venus—Rift-related, centralized volcanism and the emplacement of large-volume flow units: Journal of Geophysical Research, v. 97, no. E8, p. 15,991–16,015.

McGill, G.E., 1994, Hotspot evolution and venusian tectonic style: Journal of Geophysical Research, v. 99, no. E11, p. 23,149–23,161.

McGovern, P.J., 1996, Studies of large volcanoes on the terrestrial planets—Implications for stress state, tectonics, structural evolution, and moat filling: Ph.D. dissertation, Cambridge, Massachusetts Institute of Technology.

McKinnon, W.B., Zahnle, K.J., Ivanov, B.A., and Melosh, H.J., 1997, Cratering on Venus—Models and observations, *in* Bougher, S.W., Hunten, D.M., and Phillips, R.J. (eds.), Venus II: Tucson, University of Arizona Press, p. 969–1014.

Namiki, N., and Solomon, S.C., 1994, Impact crater densities on volcanoes and coronae on Venus—Implications for volcanic resurfacing: Science, v. 265, no. 5174, p. 929–933.

Parker, T.J., Komatsu, G., Baker, V., Gulick, V., Saunders, R., Weitz, C., and Head, J., 1991, An outflow channel in Lada Terra, Venus (abs.), *in* Lunar and Planetary Science Conference XXII: Houston, Lunar and Planetary Institute, p. 1035–1036.

Pavri, B., Head, J.W., Klose, K.B., and Wilson, L., 1992, Steep-sided domes on Venus–Characteristics, geologic setting, and eruption conditions from Magellan data: Journal of Geophysical Research, v. 97, no. E8, p. 13,455–13,478.

Phillips, R.J., Raubertas, R.F., Arvidson, R.E., Sarkar, I.C., Herrick, R.R., Izenberg, N., and Grimm, R.E., 1992, Impact craters and Venus resurfacing history: Journal of Geophysical Research, v. 97, no E10, p. 15,923–15,948.

Planetary Data System, 1993, Magellan—Altimetry and radiometry composite data: Planetary Data System, Pasadena, Jet Propulsion Laboratory [CD-ROM].

Price, M.H., Watson, G., Suppe, J., and Brankman, C., 1996, Dating of volcanism and rifting on Venus using impact crater densities: Journal of Geophysical Research, v. 101, no. E2, p. 4657–4671.

Rosenberg, L., 1995, Areal geology of the Pandrosos Dorsa quadrangle (V–5), Venus (abs.), *in* Lunar and Planetary Science Conference XXVI: Houston, Lunar and Planetary Institute, p. 1185–1186.

Sandwell, D.T., and Schubert, G., 1992a, Flexural ridges, trenches, and outer rises around coronae on Venus: Journal of Geophysical Research, v. 97, no. E10, p. 16,069–16,083.

———1992b, Evidence for retrograde lithospheric subduction on Venus: Science, v. 257, no. 5071, p. 766–770.

Schaber, G.G., Kirk, R.L., and Strom, R.G., 1995, Database of impact craters on Venus based on analysis of Magellan radar images and altimetry data (1990–1994): U.S. Geological Survey Open-File Report 95–561, 26 p.

Schaber, G.G., Strom, R.G., Moore, H.J., Soderblom, L.A., Kirk, R.L., Chadwick, D.J., Dawson, D.D., Gaddis, L.R., Boyce, J.M., and Russel, J., 1992, Geology and distribution of impact craters on Venus—What are they telling us?: Journal of Geophysical Research, v. 97, no. E8, p. 13,257–13,301.

Schultz, P.H., 1992, Atmospheric effects on ejecta emplacement and crater formation on Venus from Magellan: Journal of Geophysical Research, v. 97, no. E10, p. 16,183–16,248.

Solomon, S.C., McGovern, P.J., Simmons, M., and Head, J.W., 1994, Gravity anomalies over volcanoes on Venus—Implications for lithospheric thickness and volcano history (abs.), *in* Lunar and Planetary Science Conference XXV: Houston, Lunar and Planetary Institute, p. 1317–1318.

Squyres, S.W., Janes, D.M., Baer, G., Bindschadler, D.L., Schubert, G., Sharpton, V.L., and Stofan, E.R., 1992a, The morphology and evolution of coronae on Venus: Journal of Geophysical Research, v. 97, no. E8, p. 13,611–13,634.

Squyres, S.W., Jankowski, D.G., Simons, M., Solomon, S.C., Hager, B.H., and McGill, G.E., 1992b, Plains tectonism on Venus—The deformation belts of Lavinia Planitia: Journal of Geophysical Research, v. 97, no. E8, p. 13,579–13,599.

Stofan, E.R., Anderson, S.W., Crown, D.A., and Plaut, J.J., 2000, Emplacement and composition of steep-sided domes on Venus: Journal of Geophysical Research, v. 105, no. E11, p. 26,757–26,771.

Stofan, E.R., Sharpton, V.L., Schubert, G., Baer, G., Bindschadler, D.L., Janes, D.M., and Squyres, S.W., 1992, Global distribution and characteristics of coronae and related features on Venus—Implications for origin and relation to mantle processes: Journal of Geophysical Research, v. 97, no. E8, p. 13,347–13,378.

Tanaka, K.L. (compiler), 1994, The Venus geologic mappers' handbook: U.S. Geological Survey Open-File Report 94–438.

SYMBOLS FOR STRUCTURE/VOLCANO MAP

- Fault or lineament
- Channel or sinuous rille
- Chain craters or collapsed lava tube
- Caldera
- Small pit
- Dome (> 2 km) or circular scarp—Hachures point downslope
- Volcano without pit(s) (< 2 km)
- Volcano with pit(s) (< 2 km)
- Steep-sides volcano or structure without pit(s) (< 2 km)
- Steep-sides volcano or structure with pit(s) (< 2 km)
- Flow front—Arrow indicates flow direction
- Depression
- Crater rim crest and central peak—Dotted where buried
- Graben
- Thrust fault or ramp—Sawteeth on upper plate
- Ridge crest
- Wrinkle ridge
- Trough or narrow depression
- Basal scarp—Hachures at top of scarp point downslope

TABLE 1. *Map unit radar properties.*

[Radar map properties derived using the Venus Ancillary Data Program [Campbell, 1994]. Unit: Geologic map unit sampled. Location: Descriptive location of sample (for craters, note that interior or flow material is sampled, depending on the unit). Latitude: Measured in degrees, with northernmost latitude first and southernmost latitude second. Longitude: Measured in °E, with westernmost longitude first and easternmost second. Inc.: Radar incidence angle; where two incidence angles are listed for a given location, radar data were available from Cycle 1 left-looking and Cycle 2 right-looking; note that only SAR echo changes as a function of incidence angle. Radius: Mean, minimum, and maximum planetary radius. SAR echo: Mean, minimum, and maximum SAR echo in dB (NA indicates that minimum values were not computed by the Ancillary Data Program and are not available). RMS Slope: RMS meter-scale slope in degrees. Reflectivity: Fresnel reflectivity expressed as the power reflection coefficient. Emiss.: Microwave emissivity. $ε_s$: Probable extreme dielectric constant for a smooth surface. $ε_r$: Probable extreme dielectric constant for a rough surface]

Unit	Location	Latitude	Longitude	Inc.	Radius (km)	SAR Echo	RMS	Refl.	Emiss.	$ε_s$, $ε_r$
b	middle	−43.08 −43.16	22.27 22.46	26	6051.917 6051.68 6052.076	−3.655 NA −0.123	5 4.1 5.6	0.116 0.1 0.13	0.852 0.849 0.856	4.2, 5
b	middle	−43.08 −43.16	22.27 22.46	25		−5.599 −18.007 −2.715				
b	north	−38.48 −38.54	15.00 15.22	28	6052.045 6051.86 6052.189	−8.495 −10.337 −7.205	4.95 3.6 5.8	0.104 0.085 0.125	0.867 0.863 0.871	3.8, 4.6
b	north	−38.48 −38.54	15.00 15.22	25		−8.491 −10.503 −7.122				
b	south	−48.70 −48.75	27.54 27.64	24	6051.898 6051.876 6051.943	−6.73 −11.306 −4.552	4.33 4 4.6	0.095 0.09 0.1 0.886	0.888 0.89	3.5, 4
b	south	−48.70 −48.75	27.54 27.64	25		−5.68 −12.847 −3.109				
ci	Muriel	−41.69 −41.71	12.35 12.40	27	6052.187 6052.142 6052.227	−9.827 −11.498 −8.624	2.65 2.2 3.1	0.082 0.075 0.09	0.849 0.848 0.85	4.3, 5.1
ci	Muriel	−41.69 −41.71	12.35 12.40	25		−9.58 −14.983 −7.246				
ci	Sophia	−28.60 −28.64	18.82 18.85	34	6051.731 6051.715 6051.747	−13.859 −19.891 −11.427	1.95 1.7 2.2	0.104 0.1 0.105	0.848 0.857 0.858	3.7, 4.8
ci	Zenobia	−29.31 −29.36	28.62 28.70	33	6051.206 6051.181 6051.278	−11.007 −12.163 −10.096	2.59 2.1 3	0.11 0.1 0.115	0.87 0.868 0.871	3.4, 4.4
cf	Muriel	−41.71 −41.73	12.52 12.56	27	6052.354 6052.317 6052.392	−6.009 −7.462 −4.922	3.3 3.3 3.3	0.09 0.085 0.095	0.85 0.85 0.85	4.3, 5.1
cf	Muriel	−41.71 −41.73	12.52 12.56	25		−3.537 −25.592 −0.54				
cf	Stuart	−30.56 −30.61	20.19 20.35	32	6051.069 6051.045 6051.101	−8.294 −9.702 −7.232	1.74 1.5 2.1	0.162 0.13 0.22	0.729 0.707 0.751	7.4, 10
cf	Zenobia	−29.03 −29.09	28.66 28.76	33	6051.825 6051.815 6051.857	−9.046 −10.677 −7.864	1.25 1 1.7	0.084 0.08 0.095	0.865 0.863 0.868	3.5, 4.6
fCT	N	−35.09 −35.20	3.78 3.92	30	6051.777 6051.545 6051.873	−9.286 −10.601 −8.278	3.15 2.9 3.3	0.075 0.07 0.08	0.865 0.863 0.866	3.7, 4.6
fCT	S	−38.40 −38.61	0.31 0.69	28	6051.628 6051.597 6051.668	−11.634 −13.153 −10.51	2.36 1.6 2.7	0.135 0.12 0.16	0.865 0.863 0.866	3.8, 4.6
fCT	mid	−35.73 −35.78	19.50 19.60	30	6051.983 6051.963 6051.991	−12.014 −13.878 −10.714	2.6 2.3 3	0.143 0.14 0.145	0.831 0.831 0.831	4.6, 5.7
fd	E	−40.06 −40.29	21.43 22.00	27	6051.787 6051.717 6051.855	−10.281 −12.132 −8.987	3.12 2.2 4.2	0.135 0.1 0.15	0.836 0.829 0.842	4.6, 5.6
fd	E	−40.06 −40.29	21.43 22.00	25		−10.271 −12.269 −8.908				
fd	W	−38.08 −38.15	0.58 0.73	28	6051.561 6051.524 6051.639	−7.935 −8.937 −7.121	3.39 3 3.7	0.098 0.095 0.1	0.876 0.873 0.879	3.6, 4.3
fd	mid	−37.85 −37.92	8.23 8.61	29	6051.959 6051.937 6051.983	−8.366 −9.402 −7.53	3.33 1.7 4.6	0.113 0.09 0.13	0.853 0.85 0.854	4.1, 5
fN		−38.17 −38.28	23.20 23.42	28	6052.453 6052.317 6052.612	−10.254 −11.48 −9.299	2.74 1 5	0.095 0.07 0.125	0.858 0.856 0.859	4, 4.9
fN		−38.17 −38.28	23.20 23.42	25		−9.26 −10.563 −8.259				
fNP	NE	−36.07 −36.19	26.46 26.91	29	6052.021 6051.967 6052.133	−12.348 −13.669 −11.337	3.07 2.7 3.8	0.109 0.095 0.12	0.854 0.85 0.859	4, 5
fNP	Pachamama	−35.69 −35.74	21.57 21.66	30	6051.768 6051.722 6051.838	−12.867 −14.136 −11.887	2.4 2.2 2.7	0.116 0.11 0.125	0.844 0.843 0.844	4.2, 5.3
fNP	SE	−38.64 −38.84	25.07 25.53	28	6052.021 6051.989 6052.047	−9.667 −10.634 −8.876	3.06 2.5 3.8	0.195 0.15 0.24	0.808 0.805 0.818	5.3, 6.5
fNP	SE	−38.64 −38.84	25.07 25.53	25		−8.706 −9.958 −7.735				
fP		−35.89 −35.93	21.36 21.42	30	6051.78 6051.717 6051.843	−9.429 −11.005 −8.274	2.73 2.2 3.2	0.105 0.095 0.115	0.843 0.842 0.844	4.3, 5.3
fS	W	−42.49 −42.54	27.82 27.99	26	6052.008 6051.984 6052.02	−8.229 −9.72 −7.121	4.83 4 6.2	0.182 0.16 0.235	0.835 0.829 0.84	4.7, 5.6
fS	W	−42.49 −42.54	27.82 27.99	25		−9.657 −11.418 −8.407				
fS	E	−42.65 −42.77	28.59 28.86	26	6051.968 6051.944 6051.977	−8.229 −9.72 −7.121	2.1 2 2.2	0.139 0.13 0.15	0.807 0.804 0.812	5.5, 6.6
fS	E	−42.65 −42.77	28.59 28.86	25		−9.657 −11.418 −8.407				
fS	N	−42.49 −42.52	3.84 3.89	26	6051.718 6051.655 6051.756	−12.645 −13.742 −11.769	3.07 2.9 3.3	0.145 0.145 0.145	0.853 0.852 0.854	4.2, 5
fS	S	−44.12 −44.18	5.16 5.26	26	6051.74 6051.573 6051.976	−12.369 −14.085 −11.142	3.59 3.4 3.8	0.124 0.115 0.13	0.864 0.863 0.864	4, 4.7
f	center	−39.32 −39.35	13.22 13.26	28	6052.362 6052.349 6052.375	−11.401 −12.335 −10.633	1.35 1.3 1.4	0.166 0.155 0.175	0.819 0.818 0.82	5, 6.1
fSM_1	N	−42.21 −42.69	26.26 27.45	26	6051.979 6051.928 6052.02	−10.567 −11.59 −9.74	2.43 1.6 3.1	0.144 0.11 0.17	0.804 0.793 0.824	5.5, 6.7
fSM_1	N	−42.21 −42.69	26.26 27.45	25		−10.663 −11.983 −9.653				
fSM_1	S	−43.83 −44.00	26.37 27.04	26	6051.914 6051.875 6051.956	−10.688 −11.643 −9.905	2.19 1.8 2.8	0.096 0.09 0.1	0.854 0.847 0.864	4.2, 5
fSM_1	S	−43.83 −44.00	26.37 27.04	25		−10.692 −11.97 −9.705				
fSM_1	flow/slump?	−40.86 −41.00	21.32 21.61	27	6051.712 6051.678 6051.743	−10.653 −11.7 −9.81	2.2 1.7 2.6	0.136 0.125 0.1	0.817 0.813 0.824	5.1, 6.2
fSM_1	flow/slump?	−40.86 −41.00	21.32 21.61	25		−10.583 −11.899 −9.574				
fUA	E	−48.62 −49.12	27.77 28.81	24	6051.75 6050 6052.185	−4.826 −5.771 −4.05	5.55 3.8 9.1	0.093 0.07 0.17	0.898 0.892 0.902	3.3, 3.7
fUA	E	−48.62 −49.12	27.77 28.81	25		−5.468 −6.917 −4.384				
fUA	W	−48.92 −49.08	18.13 18.53	24	6051.591 6051.565 6051.612	−14.619 −15.681 −13.766	1.15 0.9 1.5	0.153 0.12 0.235	0.839 0.836 0.841	4.8, 5.5
fUA	mid	−47.41 −47.50	23.44 23.90	24	6052.351 6052.279 6052.406	−9.562 −10.475 −8.809	2.07 1.6 2.4	0.138 0.13 0.15	0.821 0.819 0.823	5.2, 6.1
fUA	mid	−47.41 −47.50	23.44 23.90	25		−10.664 −11.996 −9.646				
pd	E	−39.91 −40.26	27.79 28.27	27	6052.136 6052.097 6052.2	−11.505 −12.741 −10.544	1.79 1.2 2.4	0.115 0.095 0.135	0.831 0.815 0.842	4.7, 5.7
pd	E	−39.91 −40.26	27.79 28.27	25		−11.294 −12.794 −10.181				
pd	Kaiwan	−46.54 −46.80	358.98 359.19	24	6050.665 6050.6 6050.688	−9.73 −12.719 −7.977	1.93 1.2 3.1	0.099 0.085 0.12	0.865 0.859 0.871	4, 4.7
pd	Kaiwan	−46.54 −46.80	358.98 359.19	25		−10.998 −14.301 −9.143				
pd	Vaidilute	−37.66 −38.03	14.06 14.41	29	6051.8 6051.77 6051.856	−13.966 −15.613 −12.775	2.41 1.7 2.9	0.103 0.075 0.13	0.871 0.862 0.881	3.7, 4.4
pd	Vaidilute	−37.66 −38.03	14.06 14.41	25		−13.64 −15.218 −12.485				
pdr	Carpo	−37.36 −37.41	3.52 3.72	29	6051.812 6051.511 6052.178	−8.347 −10.515 −6.908	4.29 3.6 4.9	0.083 0.075 0.09	0.881 0.878 0.883	3.5, 4.2
pdr	Selu	−42.54 −42.59	6.05 6.16	26	6052.35 6052.23 6052.595	−12.967 −14.361 −11.914	4.4 4.1 5.1	0.079 0.07 0.09	0.862 0.861 0.864	4, 4.7
pdr	Tyche	−43.44 −43.49	16.52 16.72	24	6052.184 6052.102 6052.251	−8.315 −9.589 −7.332	4.23 3.7 4.5	0.059 0.055 0.06	0.884 0.884 0.885	3.5, 4.1
pdr	Tyche	−43.44 −43.49	16.52 16.72	25		−9.209 −10.935 −7.977				
pe	Alpha	−32.20 −32.26	5.84 6.05	32	6051.926 6051.793 6052.007	−9.552 −11.017 −8.459	2.78 2.2 3.4	0.1 0.095 0.105	0.857 0.855 0.859	3.8, 4.8
pe	Dorothy	−35.06 −35.15	11.03 11.13	30	6051.84 6051.805 6051.884	−12.301 −13.91 −11.13	1.1 0.9 1.4	0.088 0.075 0.095	0.856 0.855 0.858	3.9, 4.9
pe	Holiday	−46.80 −46.89	10.55 10.68	24	6052.113 6051.94 6052.263	−11.681 NA −6.14	2.27 1.6 3.3	0.131 0.125 0.135	0.848 0.845 0.851	4.5, 5.2
pe	Holiday	−46.80 −46.89	10.55 10.68	25		−13.696 NA −8.728				
pi	Alpha-N	−27.03 −27.12	4.68 4.85	34	6052.195 6052.14 6052.277	−12.112 −13.632 −10.989	2.39 2.2 2.8	0.077 0.075 0.09	0.869 0.867 0.87	3.4, 4.5
p	Alpha-S	−29.44 −29.51	5.07 5.24	33	6052.358 6052.275 6052.415	−10.955 −12.498 −9.819	3.1 2.3 3.7	0.111 0.11 0.115	0.833 0.829 0.837	4.2, 5.6
pi	Tyche	−44.20 −44.22	13.78 13.90	26	6051.674 6051.644 6051.687	−11.329 −12.742 −10.265	1.07 1 1.2	0.05 0.05 0.05	0.899 0.898 0.9	3.2, 3.7
pi	Tyche	−44.20 −44.22	13.78 13.90	25		−12.686 −13.956 −11.705				
pr	Alpha	−31.44 −31.55	5.12 5.32	32	6051.851 6051.831 6051.869	−12.526 −13.748 −11.573	2.26 2.1 2.9	0.074 0.07 0.075	0.887 0.884 0.89	3.2, 4
pr	E	−33.22 −33.44	7.25 7.84	31	6051.844 6051.737 6051.974	−12.791 −14.544 −11.545	1.27 0.9 1.7	0.117 0.095 0.14	0.842 0.839 0.844	4.2, 5.3
pr	mid	−34.17 −34.29	7.61 7.76	30	6051.877 6051.804 6051.92	−13.443 −14.496 −12.597	0.73 0.5 1	0.098 0.085 0.105	0.849 0.848 0.851	4, 5.1
prh	Dorothy	−37.29 −37.9	10.97 11.61	29	6051.762 6051.712 6051.821	−17.761 −18.808 −16.919	0.95 0.4 1.3	0.122 0.085 0.215	0.845 0.839 0.851	4.3, 5.3
prh	Dorothy	−37.29 −37.91	10.97 11.61	25		−17.404 −18.744 −16.382				
prh	N	−33.49 −33.82	13.13 13.53	31	6051.857 6051.823 6051.883	−19.626 −20.595 −18.835	1.27 0.9 1.6	0.111 0.095 0.125	0.854 0.851 0.859	3.9, 4.9
prh	Ninhu	−39.47 −39.65	22.95 23.31	28	6051.903 6051.869 6051.918	−12.123 −13.076 −11.342	2.29 1.7 2.6	0.151 0.125 0.175	0.816 0.813 0.824	5.1, 6.2
prh	Ninhu	−39.47 −39.65	22.95 23.31	25		−12.49 −13.709 −11.538				
prl	~corona feature	−30.29 −30.34	9.50 9.59	33	6051.719 6051.705 6051.735	−11.406 −13.184 −10.148	1.92 1.7 2.1	0.09 0.09 0.09	0.844 0.843 0.844	4, 5.2
prl	SW	−44.29 −44.82	4.85 5.14	25	6051.391 6051.304 6051.49	−16.693 −17.67 −15.896	1.54 1.1 2.1	0.112 0.1 0.12	0.866 0.864 0.869	4, 4.6
prl	Stuart	−28.93 −29.09	20.62 20.81	33	6051.752 6051.711 6051.804	−20.408 −21.569 −19.492	1.13 0.8 1.4	0.127 0.115 0.145	0.858 0.857 0.859	3.7, 4.8
prl	Woolf	−38.14 −38.21	27.42 27.61	2	6051.986 6051.969 6052.006	−11.841 −12.991 −10.933	1.54 1.2 1.8	0.111 0.095 0.135	0.858 0.857 0.859	4, 4.8
prl	Woolf	−38.14 −38.21	27.42 27.61	25		−11.014 −12.374 −9.979				
prt	Alpha	−29.65 −30.13	1.03 1.50	33	6052.979 6052.788 6053.111	−11.252 −12.657 −10.192	3.1 1.7 4.8	0.137 0.105 0.16	0.829 0.825 0.835	4.3, 5.7
prt	E	−35.16 −35.19	29.84 29.95	30	6052.561 6052.536 6052.579	−9.5 −11.636 −8.074	5.5 5.4 5.6	0.104 0.095 0.11	0.875 0.874 0.876	3.5, 4.3
prt	mid	−34.11 −34.18	8.49 8.64	30	6052.076 6051.966 6052.155	−10.634 −12.14 −9.519	1.72 1.2 2.2	0.072 0.07 0.08	0.848 0.848 0.849	4.1, 5.1
prt	SE	−49.46 −49.58	29.46 29.74	23	6052.147 6052.023 6052.275	−11.58 −14.275 −9.929	2.01 1.6 2.3	0.079 0.07 0.095	0.877 0.871 0.884	3.8, 4.3
ptt	Alpha	−31.42 −31.47	9.74 9.80	32	6052.038 6051.932 6052.185	−13.347 −14.678 −12.33	2.03 2 2.1	0.117 0.105 0.125	0.846 0.844 0.849	4, 5.2
ptt	dome105	−31.81 −31.84	10.43 10.48	32	6051.844 6051.819 6051.87	−12.729 −14.146 −11.663	0.62 0.4 0.9	0.112 0.085 0.135	0.831 0.83 0.831	4.4, 5.7
ptt	mid	−36.52 −36.56	18.73 18.88	29	6051.964 6051.958 6051.972	−11.434 −12.548 −10.547	1.98 1.7 2.3	0.156 0.135 0.175	0.828 0.825 0.83	4.7, 5.8
t	Alpha-E	−26.69 −26.82	7.19 7.41	35	6053.709 6053.246 6053.969	−5.739 NA −2.142	4.6 3.5 6.6	0.101 0.09 0.125	0.858 0.853 0.861	3.6, 4.8
t	Alpha-W	−26.84 −27.04	2.54 2.84	34	6053.183 6052.126 6053.663	−7.26 NA −3.703	4.37 3.1 6.5	0.067 0.06 0.0	0.871 0.863 0.878	3.4, 4.4
t	Tyche	−42.88 −42.96	13.49 13.67	26	6051.861 6051.697 6052.043	−5.707 −10.225 −3.541	4.14 3 5.3	0.056 0.05 0.065	0.916 0.914 0.918	2.8, 3.3
t	Tyche	−42.88 −42.96	13.49 13.67	25		−7.246 −12.15 −5.001				
va	Alpha	−29.09 −29.1	9.80 9.91	33	6051.78 6051.773 6051.791	−15.799 −19.926 −13.722	1.26 1.1 1.5	0.142 0.115 0.16	0.84 0.839 0.84	4.1, 5.4
va	S	−37.39 -37.57	12.63 12.93	29	6051.884 6051.853 6051.95	−14.629 −17.677 −12.855	1.53 0.9 2.1	0.13 0.09 2.1	0.858 0.855 0.859	4, 4.8
va	mid	−34.36 −34.50	15.14 15.33	30	6052.063 6052.011 6052.111	−18.424 −20.014 −17.263	3.13 2.4 3.5	0.114 0.105 0.13	0.857 0.855 0.858	3.9, 4.9
vd	dome102	−29.71 −29.75	12.07 12.11	33	6051.878 6051.858 6051.899	−15.685 −19.099 −13.797	0.5 0.4 0.6	0.095 0.095 0.095	0.833 0.832 0.833	4.3, 5.6
vd	dome103	−29.71 −29.77	12.22 12.28	33	6052.141 6051.919 6052.29	−13.366 −17.653 −11.251	1.12 0.6 1.8	0.096 0.085 0.105	0.834 0.833 0.835	4.2, 5.6
vd	dome105	−32.01 −32.07	10.27 10.36	32	6051.966	−12.293	1.55	0.062	0.833	4.3, 5.6
vs	N	−37.46 −37.57	13.37 13.46	29	6051.908 6051.85 6051.964 6051.796 6052.287	−11.482 −12.777 −10.486 −14.955 −10.655	2.38 2 2.6 0.9 2	0.095 0.09 0.1 0.055 0.085	0.847 0.846 0.847 0.831 0.835	4.2, 5.2
vs	S	−38.03 −38.08	12.77 12.88	28	6051.787 6051.764 6051.796	−12.23 −13.625 −11.176	1.47 1.1 1.9	0.094 0.09 0.095	0.853 0.852 0.854	4.1, 5

ISBN 0-607-98059-1
9 780607 980592

Any use of trade, product, or firm names in this publication is for descriptive purposes only and does not imply endorsement by the U.S. Government

For sale by U.S. Geological Survey, Information Services, Box 25286, Federal Center, Denver, CO 80225, 1–888–ASK–USGS

Printed on recycled paper